

A Computational Analysis of the Application of Skewness and Kurtosis to Corrugated and Abraded Surfaces

Authors:

T.J.G. Downey¹

P. Martin¹

M. Sedlaček²

L.Y. Beaulieu^{1,3}

Affiliations:

1 *Department of Physics and Physical Oceanography, Memorial University of Newfoundland, St. John's, NL, Canada*

2 *Institute of metals and technology, Ljubljana, Slovenia*

3 *Corresponding author:*

E-mail: lbeaulieu@mun.ca

Abstract

We investigate the use of skewness and kurtosis for characterizing the morphology of abraded surfaces consisting of scratches and corrugated surfaces composed of hemispherical grains. Skewness and kurtosis were found to be ineffective at characterizing corrugated surfaces which were best described using the RMS roughness, RMS slope, and surface area ratio. Corrugated surfaces with RMS roughness values differing by a factor of 5 exhibited near constant values of skewness and kurtosis. Abraded surfaces, in contrast, produced nearly constant values of RMS roughness, RMS slope, and surface area ratio while the skewness and kurtosis varied significantly. Hence abraded surfaces were found to be well characterized by the skewness and kurtosis leading to a simple relationship with the number of scratches.

1. Introduction

In the nineteenth century, it was common practice to use the normal distribution (ND) to describe any data set which had a reasonably high degree of symmetry¹. Pearson, however, observed that the deviation of data from the ND was, in some cases, very large. He therefore created two statistical parameters to quantify how a distribution deviated from the ND²⁻⁶. The skewness S_{sk} is defined as

$$S_{sk} = \frac{1}{N\sigma^3} \sum_{i=1}^N (z_i - \mu)^3, \quad (1)$$

where z_i are the data points, μ is the mean value of the data, N is the number of data points, and σ is the standard deviation. Skewness (S_{sk}), also known as the third moment of the distribution, is used to quantify the level of asymmetry in a distribution. Skewness is negative when there is a preponderance of large data values causing the distribution to appear to have a long flat tail for smaller values. Conversely, a positive distribution is produced from data dominated by smaller values. A skewness of zero generally indicates that the distribution is symmetric about the mean. The kurtosis S_{ku} is defined as

$$S_{ku} = \frac{1}{N\sigma^4} \sum_{i=1}^N (z_i - \mu)^4, \quad (2)$$

where the symbols have the same meaning as above, and indicates the level of flatness or sharpness of the distribution. Kurtosis also known as the fourth moment of the distribution, is less than 3 when the distribution has a shorter and flatter peak compared to the ND (also called platykurtic) and is greater than 3 when the distribution has a longer and sharper peak (leptokurtic) when compared to the ND. Lastly, the kurtosis is equal to 3 for the case of a normal distribution.

Skewness and kurtosis are used in a number of fields, including surface metrology

and characterization^{7,8}, tribology⁹⁻¹², and dental science^{13,14}. The majority of the literature has largely been confined to discussions of flat surfaces with abrasions such as human teeth or mechanical parts suffering from wear^{9,14}. The use of skewness and kurtosis for characterizing surfaces composed of hemispherical particles has not yet been thoroughly investigated.

In this paper, we investigate the applicability of the skewness and kurtosis for characterizing surfaces composed of hemispherical grains as is typically produced by sputter deposition and contrast those to the more well-known application of abraded surfaces. This work is motivated by recent attempts to correlate the sensitivity of cantilever sensors to the roughness of the Au film used to immobilize the sensing layer on a silicon cantilever. To date, researchers have used, almost exclusively, the root-mean-squared (RMS) roughness for characterizing these surfaces however this parameter only provides the standard deviation of the surface height^{7,9,10,13,14}. There is a clear need to better describe these surfaces to obtain a clearer understanding of the relationship between the surface topography of the Au film to the sensitivity of cantilever sensors.

2. Computational Details

To generate specific surfaces, a program was written to produce surfaces composed of hemispherical features and flat surfaces with scratch patterns. The corrugated surfaces were generated by first creating a two-dimensional grid. On each grid point (x_i, y_j) , an inverted paraboloid, as defined in equation 3, was created to simulate the hemispherical grains.

$$z(x, y) = c \left(\frac{(x-x_i)^2}{a^2} + \frac{(y-y_j)^2}{b^2} \right) + z_0, \quad c < 0 \quad (3)$$

The shape of the inverted paraboloid was controlled by the parameters a, b, c , and z_0 where a and b control the level of curvature

along the x and y direction, c controls the elongation, and z_o sets the base height of the paraboloid. In all cases a was set equal to b to ensure that the particles appeared spherical. In order to reproduce actual surfaces as best as possible, each parameter in equation 3 was

allowed to fluctuate between 0 - 20%. An example of a simulated surface is shown in fig. 1a and compared to an image taken by atomic force microscopy of an actual Au surface shown in figure 1b. As can be seen the two surfaces are strikingly similar.

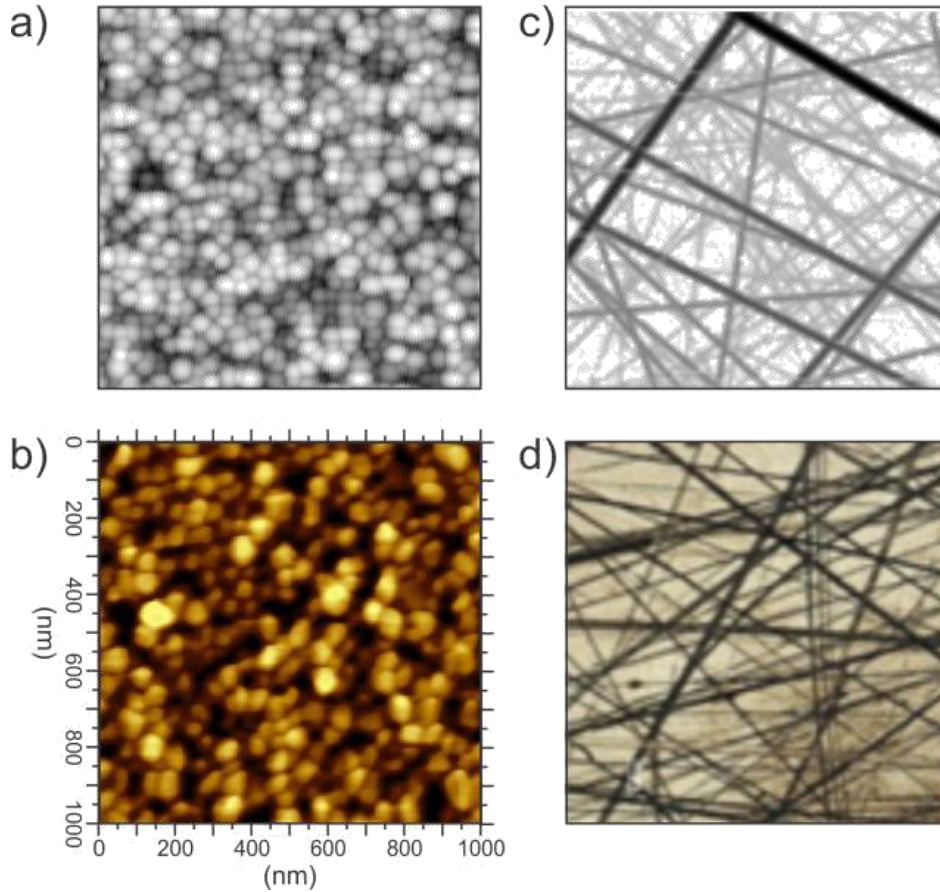


Figure 1: a) A surface image from the corrugated surface simulation. b) An AFM image of a gold film produced by sputter deposition. The colour contrast scale from dark (low points) to light (high points) represents a height change of 19 nm. c) Simulated abraded surface with 210 scratches; d) An optical image of abraded 100Cr6 (AISI 52100) ball bearing steel.

Surfaces with scratches were simulated starting with a flat surface ($z = 0$). Each scratch was defined by a half cylinder of radius r embedded in the surface such that the central axis of the cylinder remained in the $z = 0$ plane. The direction and position of each scratch were chosen at random and were defined by a vector \vec{N} normal to the central

axis and lying in the $z = 0$ plane and a point \vec{p} on the central axis respectively. The depth, z , at each point \vec{a} of the scratch was defined by $z = -\sqrt{r^2 - L^2}$ where L is given by equation 4¹⁵:

$$L = \frac{\vec{N} \cdot (\vec{a} - \vec{p})}{\|\vec{N}\|}. \quad (4)$$

This definition for z ensures that only values of \vec{a} for which $r^2 > L^2$ are used to define the scratch. The scratches are then distributed across the surface using a user-defined distribution of coarse, medium, fine, and superfine scratches. As can be seen in fig. 1, the surfaces created by our algorithm shown in fig. 1c appear remarkably similar to the optical image taken of an actual abraded surface shown in fig. 1d.

To calculate the roughness parameters of a surface, the primary profile of the surface must first be filtered to separate the waviness and roughness profiles (see fig. 2). This is accomplished by convolving a matrix containing the 2D surface data, z_{ij} , with a

Gaussian weighting matrix, whose entries are given by equation 5¹⁶,

$$h_{ij} = \frac{1}{\alpha\lambda_c} e^{-\pi\left(\frac{z_{ij}}{\alpha\lambda_c}\right)^2}, \quad (5)$$

where $\alpha = \sqrt{\frac{\ln(2)}{\pi}}$, and λ_c is the filter cut-off wavelength. The matrix convolution is accomplished through the use of a Fast Fourier Transform (FFT) by means of the Convolution Theorem,

$$h_{ij} * z_{ij} = \mathcal{F}^{-1}\left(\mathcal{F}(h_{ij}) \cdot \mathcal{F}(z_{ij})\right), \quad (6)$$

where $*$ denotes the convolution operator, and \mathcal{F} and \mathcal{F}^{-1} denote the FFT and inverse FFT respectively.

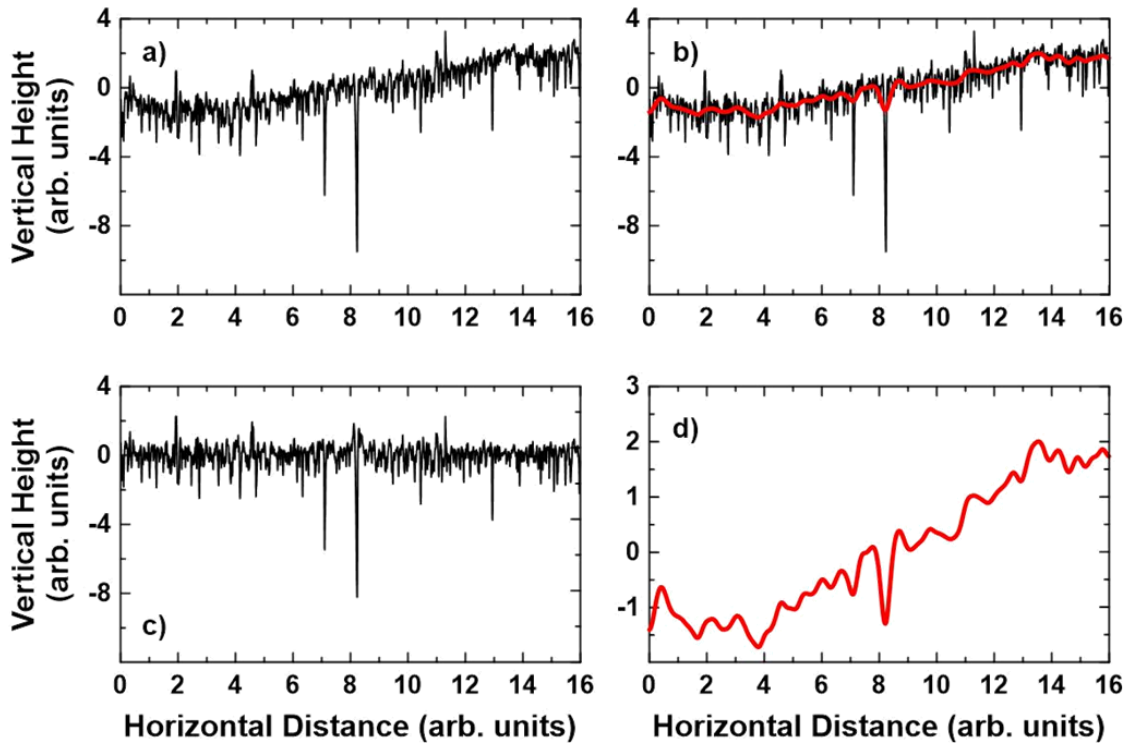


Figure 2: a) The primary surface profile is b) fitted with a weighted Gaussian moving average (red line) called the waviness profile. The primary profile is split into the c) roughness and d) waviness profiles by taking the difference of the primary and roughness profiles.

After the surface was filtered, it is was characterized by calculating the skewness and kurtosis as defined above as well as the RMS roughness, S_q , the surface area ratio, S_{dr} , and the RMS slope, S_{dq} , as defined elsewhere¹⁷. Because the surfaces were created with an initial set of parameters which were then randomized within a percent range, each surface with the given set of initial parameters (defined in equations 3 and 4) plus fluctuations was created ten times and the average values of the surface characterization parameters listed above were calculated and reported below. The error bars show the average of the maximum and minimum value obtained for each parameter.

3. Results

For corrugated surfaces, it is useful to plot the statistical parameters against the a parameter (from equation 3) normalized with respect to the average nearest neighbour distance (NND). We define $NND = \frac{\sqrt{N}}{g}$, where N is the number of particles on the surface and g is the grid size. Thus, we define the dimensionless quantity $a^* = \frac{a}{NND}$. Figure 3a shows the RMS roughness (blue), RMS slope (black), surface area ratio (red), kurtosis (green), and skewness (purple) plotted for corrugated surfaces as a function of the parameter a^* . As a^* increases the hemispherical surface features become broad and flat. The data in figure 3a is shown for four different values of c which defines the vertical elongation of the particles. Therefore the hemispherical surface features with $c = 70$ will be longer than those defined with $c = 10$. As can be seen, the RMS roughness, RMS slope, and surface area ratio all increase with decreasing values of a^* and also increase with increasing c . This result is not surprising since the parameter a^* controls the in-plane particle size while the c parameter controls the elongation of the hemispherical particles causing the surface to become rougher and

surface area to become larger. In contrast to these parameters the kurtosis and skewness remain constant with changes in both a^* and c . This is because the shape of the distribution is affected little for these types of surfaces. Typically the distribution of hemispherical surfaces is skewed to the left causing the skewness to consistently be negative. This also causes the distributions to be slightly wider than the normal distribution causing the kurtosis to be slightly greater than 3. Figure 3b shows the same surface characterization parameters, calculated for abraded surfaces, indicated with the same colors as in fig 3a versus the percent surface coverage of the substrate. The percent surface coverage is the ratio of the area created by the scratches divided by the initial area of the substrate. Therefore the larger the percent surface coverage the greater the number of scratches on the surface. As can be seen in fig. 3b, the RMS roughness, the RMS slope, and the surface area ratio are relatively unaffected by the number of scratches. This is because for typical scratch patterns produced by repeated abrasion through wear, the variability of the scratches is very small within the range of the smallest scratch to the largest. This is consistent with results from Sedlaček *et al*⁸. This causes the RMS roughness, RMS slope, and the surface area ratio to change very little. In contrast to these parameters, the kurtosis and skewness both show a significant change with the percent coverage.

Figure 3c, shows a plot of kurtosis vs skewness for abraded surfaces. Since the skewness and the kurtosis for abraded surfaces are both simple functions of the surface coverage, it is not surprising that kurtosis versus skewness be characterized by a simple curve as well. Although this is not a sufficient condition for the application of skewness and kurtosis, it is a necessary condition for surface characterization, and thus hints at the usefulness of these parameters.

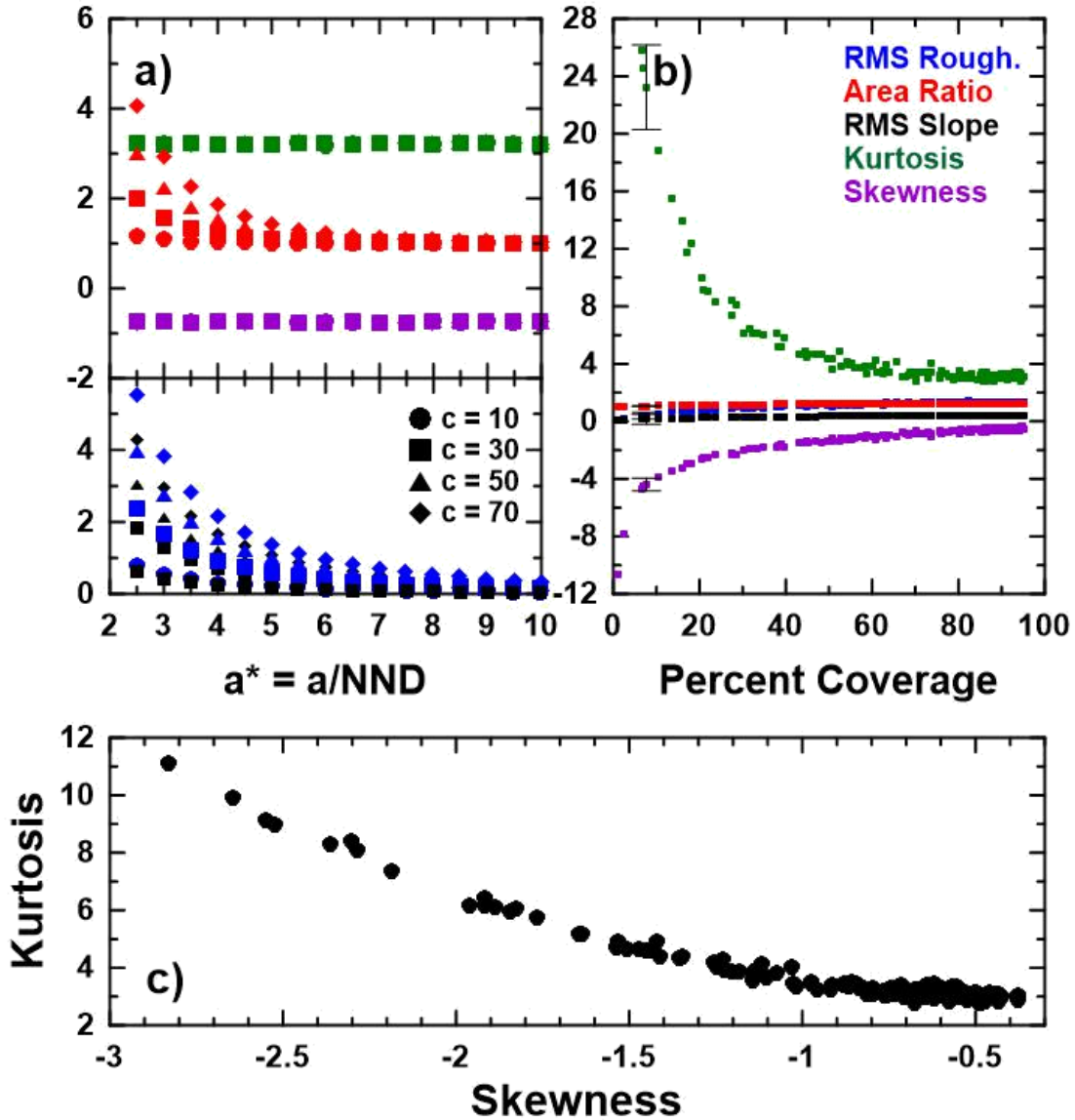


Figure 3: a) The RMS roughness (blue), RMS slope (black), surface area ratio (red), kurtosis (green) and skewness (purple) for corrugated surfaces, plotted against the parameter a^* . Circles represent $c = 10$, squares represent $c = 30$, triangles represent $c = 50$, and diamonds represent $c = 70$. b) The RMS roughness, RMS slope, surface area ratio, kurtosis, and skewness for abraded surfaces plotted against percentage surface coverage. c) Kurtosis vs skewness for abraded surfaces.

Although the surfaces analyzed in figure 3 were generated with a distribution of 5%, 10%, 25%, and 60% coarse, medium, fine, and superfine scratches, the above behaviour was observed with multiple scratch distributions. Figure 4 shows the kurtosis versus skewness for abraded surfaces with coarse, medium, fine, and superfine scratch distributions as follows: (5%, 5%, 10%, 80%),

(5%, 10%, 25%, 60%), (10%, 20%, 40%, 30%), (20%, 40%, 30%, 10%), (40%, 30%, 20%, 10%). As can be seen the kurtosis versus skewness all fall on one universal curve. With the RMS roughness displayed with color, it can be seen that the RMS roughness changes proportionally with both the kurtosis and the skewness.

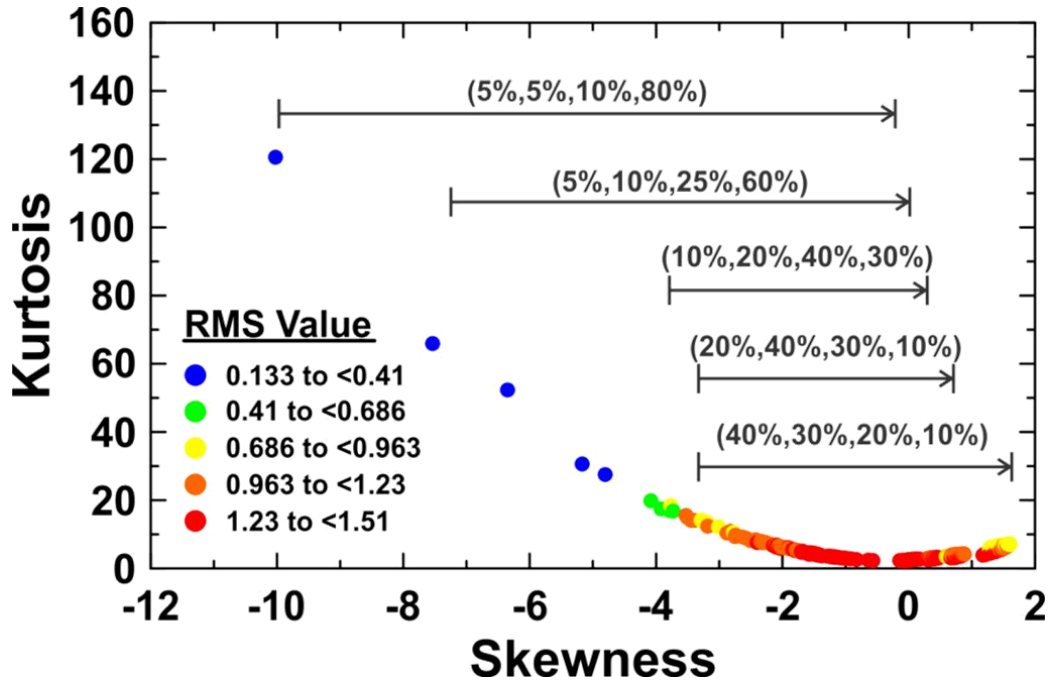


Figure 4: Kurtosis versus skewness for abraded surfaces with 5 different scratch distributions. The color of the data indicates the RMS roughness of the surfaces. The arrows indicate the direction of increased surface coverage for each scratch distribution.

4. Discussion

For corrugated surfaces the skewness and kurtosis remained constant at values of $S_{sk} \approx -1$ and $S_{ku} \approx 3$ while for abraded surfaces the skewness and kurtosis settle at values of $S_{sk} \approx 1$ and $S_{ku} \approx 3$ as the coverage goes to 100%. This behaviour is due to the fact that, as an abraded surface becomes completely covered with scratches, the surface begins to resemble an inverted corrugated surface which has a similar value of kurtosis and negative value of skewness. A comparison of the cross-sections of both an inverted abraded surface and a corrugated surface is shown in fig. 5. The above result can be understood by realizing that abraded surfaces are the intermediate step between a perfectly flat surface to a corrugated surface as interpreted by the statistical parameters S_q , S_{dr} , S_{dq} , S_{ku} , and S_{sk} . When a surface begins to be textured through wear or abrasion, the RMS roughness, RMS slope, and surface area ratio change little while the skewness and

kurtosis start from initial high negative and positive values (respectively) and begin to increase and decrease respectively. This is because the initial surface is dominated by $z = 0$ values which causes a sharp negatively skewed distribution. As the surface coverage reaches 100% the kurtosis and skewness reach a steady state. As the surface features become more pronounced the kurtosis and skewness remain approximately constant while the RMS roughness, RMS slope and the surface area ratio begin to increase in value.

5. Conclusions

This work has examined the characterization of the topography of two types of surfaces. Corrugated surfaces were found to be well characterized by the RMS roughness, surface area ratio, and RMS slope as indicators of the level of corrugation (or roughness) of each surface. These values are analogous to the grit values used to

characterize the roughness of sandpaper. The kurtosis and skewness, however, showed no direct correlation with the roughness of the corrugated surfaces and as a result were found to be poor indicators for characterizing such surfaces. In contrast, the skewness and kurtosis of abraded surfaces were found to be the key indicators for characterizing these types of surfaces which are found to differ not in terms of their roughness but instead in terms of their level of abrasion described here as the surface area coverage. Further, the variation of individual surface features does not impact the skewness or kurtosis for abraded surfaces, which supports the idea that an abraded surface can be described by its degree of surface coverage.

Because the surface characterization parameters are not a function of the in-plane distances but only a function of the surface height, the analyses presented here are applicable to any type of surface with similar surface features from thin films to orange peel surfaces of poorly painted surfaces or macro-to micro-sized abrasions.

Acknowledgement

The authors would like to thank Memorial University and NSERC for providing the funding necessary to conduct this work.

References

- ¹ Fiori, A, Zenga, M., *Int. Stat. Rev.*, **77**, 40, (2009)
- ² Pearson, K. *Phil. Trans. R. Soc. A*, **185**, 71, (1894)
- ³ Pearson K., *Phil. Trans. R. Soc. A*, **186**, 343, (1895)
- ⁴ Pearson K., *Phil. Trans. R. Soc. A*, **197**, 443, (1901)
- ⁵ Pearson K., *Phil. Trans. R. Soc. A*, **60**, 236, (1902)
- ⁶ Pearson K., *Biometrika Trust A*, **4**, 169, (1905)
- ⁷ Peltonen, J., Järn, M., Areva, S., Linden, M, Rosenholm, J., *J. Am. Chem. Soc.*, **20**, 9428, (2004)
- ⁸ İközler, B., Peker, S.M., *Thin Solid Films*, **558**, 149, (2014)
- ⁹ Sedlaček, M., Podgornik B., Vizintin, J., *Tribol. Int.*, **48**, 102 (2012)
- ¹⁰ Sedlaček, M., Vilhena L.M.S., Podgornik B., Vizintin, J. *J. Mech. Eng.*, **57**, 674, (2011)
- ¹¹ Tayebi, N., Polycarpou, A.A., *Tribol. Int.*, **37**, 491, (2004)
- ¹² Liu X., Chetwynd D.G., Gardner J.W., *Int. J. Mach. Tool Manu.*, **38**, 669, (1998)
- ¹³ Hansson K.N., Hansson S., *ISRN. Mater. Sci*, 2011, (2011)
- ¹⁴ Meireles A.B., de Souza Bastos, F., Cornacchia T.P., Ferreria J.A., de Las Casas E.B., *Biotribology*, 1-2, pp 35-41, (2015)
- ¹⁵ Farin G. Hansford D., *Practical Linear Algebra: A Geometry Toolbox*, Ch. 3, Pg. 44, *A.K. Peters Ltd.*, (2004)
- ¹⁶ Yuan, Y.B, Vorburger, V.B, Song, J.F, Renegar, T.B, *X International Colloquium on Surfaces*, p.133, (2000)
- ¹⁷ Gadelmawla E.S., Koura M.M., Maksoud T.M.A., Elewa L.M., Soliman H.H., *J. Mater. Process. Tech.*, **123**, 133, (2002)